INL/CON-09-17404
PREPRINT

Natural Circulation Patterns in the VHTR Air-Ingress Accident and Related Issues

NUTHOS-8

Chang H. Oh
Eung S. Kim
Hyung S. Kang

October 2010

The INL is a
U.S. Department of Energy
National Laboratory
operated by
Battelle Energy Alliance

Natural Circulation Patterns in the VHTR Air-Ingress Accident and Related Issues

Chang H. Oh, Eung S. Kim, and Hyung S. Kang
Idaho National Laboratory
P.O. Box 1625
Idaho Falls, ID.83415-3870
Chang.Oh@inl.gov

ABSTRACT

Natural circulation patterns in the VHTR during a hypothetical air-ingress accident have been investigated using computational fluid dynamic (CFD) methods in order to compare results from the previous 1-D model which was developed using GAMMA code for the air-ingress analyses. The GT-MHR 600 MWt reactor was selected to be the reference design and modeled by a half symmetric 3-D geometry using FLUENT 6.3, a commercial CFD code. CFD simulations were carried out as the steady-state calculation, and the boundary conditions were either assumed or provided from the 1-D GAMMA code results. Totally, 12 different cases have been reviewed, and many notable results have been obtained through in this work. According to the simulations, natural circulation patterns in the reactor were quite different from the previous 1-D assumptions. A large re-circulation flow with thermal stratification phenomena was clearly observed in the hot-leg and the lower plenum in the 3-D model. This re-circulation flow provided about an order faster air-ingress speed (0.46 m/s in superficial velocity) than previously predicted by 1-D modeling (0.02~0.03 m/s). It indicates that the 1-D air-ingress modeling may significantly distort the air-ingress scenario and consequences. In addition, complicated natural circulation patterns are eventually expected to result in very complex graphite oxidations and corrosion behaviors.

KEYWORDS

VHTR, Air Ingress, CFD, Natural Circulation, Recirculation

1. INTRODUCTION

Currently, an air-ingress accident is considered to be one of the most important safety issues for a very high temperature gas-cooled reactor (VHTR). This accident is followed by a loss of coolant in the primary flow loop from a postulated double-ended guillotine break, the worst case. Air from the confinement will react with the reactor core and supporting rods made of graphite in the lower plenum and the graphite oxidation will accelerate heat-up of the bottom reflector and reactor core, which might results in a potential release of fission products and mechanical degradation of the supporting graphite rods. Therefore, the air-ingress scenarios and phenomena are very important in VHTR safety analyses.

Previously, the earlier air-ingress mechanism shown in the literature was considered to be controlled by molecular diffusion governed by Fick's Law (Takeda 1997, Takeda and Hishida 1996, Oh et al. 2006, Kim et al. 2007, NO et al., 2007) when one-dimensional numerical tool was used. According to those studies, the air-ingress speed is very slow and it takes a couple of days before the onset-natural-circulation (ONC) occurs. Yih (1980) predicted that the ONC will begin at 220 hours following pipe rupture by using MELCOR code. NO et al. (2007) estimated the ONC time by using GAMMA code and reported that it is between 150 and 200 hours depending on the initial air volume in the containment. Besides, many other researchers estimated the similar ranges of the ONC time.

However, it was recently reported by Idaho National Laboratory (Oh et al. 2008, Oh et al. 2009, and etc.) that the earlier scenarios based on the molecular diffusion might mislead what will occur in the real situation when the pipe or break orientations are not vertical. According to their findings, air-ingress process might not initially be controlled by the molecular diffusion process, rather by a density gradient driven stratified flow of hot helium and cold air, which generally happens when a heavy fluid (in the cavity) intrudes into a light fluid (in the lower plenum). Their calculations by computational fluid dynamics (CFD) methods showed that the ONC time can be significantly shorten within a couple of minute in the real situations (Oh et al. 2008, 2009). Based on the simulations, they also provided a new air-ingress scenario that consists of four steps; (1) depressurization, (2) stratified flow (stage 1), (3) stratified flow (stage 2), and (4) natural circulation.

This paper is focused on the flow patterns after ONC, which will affect the graphite oxidation specifically in the lower plenum because the graphite oxidation and corrosion behaviors are significantly affected by detailed natural circulation flow patterns and speeds. According to the earlier studies, the natural circulation pattern in the air-ingress accident was assumed to be a single flow path from hot leg to cold leg. By this assumption, the air-ingress accident was modeled by one dimensional geometries, and the air-ingress speeds were estimated to be around 0.1~0.2 m/s throughout the reactor. However, our recent multi-dimensional simulations described in this paper shows that this assumption based on the single flow path is incorrect. The following sections summarize our CFD works on the natural circulation in the air-ingress accident, and finally discuss some new issues.

2. THREE-DIMENSAIONAL CFD MODELIING

In this paper, CFD analyses have been performed for characterizing the natural circulation flow in the air-ingress accident. Figure 1 shows the 3-D grid model for the CFD model for the GT-MHR design. Because of the unique orientation of the inlet cross duct, the GT-MHR was modeled as a half symmetric geometry. The basic dimensions and geometries are based on the GT-MHR 600MWt reactor (Oh et al. 2008). Hexahedral meshes were separately generated by ICEM-CFD software (ANSYS 2008) for the core, the upper plenum, the coolant riser, the reactor bottom blocks and the confinement, and the lower plenum was modeled by GAMBIT with hexahedral, tetrahedral, and pyramidal meshes (Johnson 2008). All the grids generated using GAMBIT for the lower plenum and the ICEM-CFD for the rest of the geometry separately were imported into the FLUENT 6.3 and merged by using the grid interface method. Table 1 summarizes the grid information for each region in the 3-D grid model.

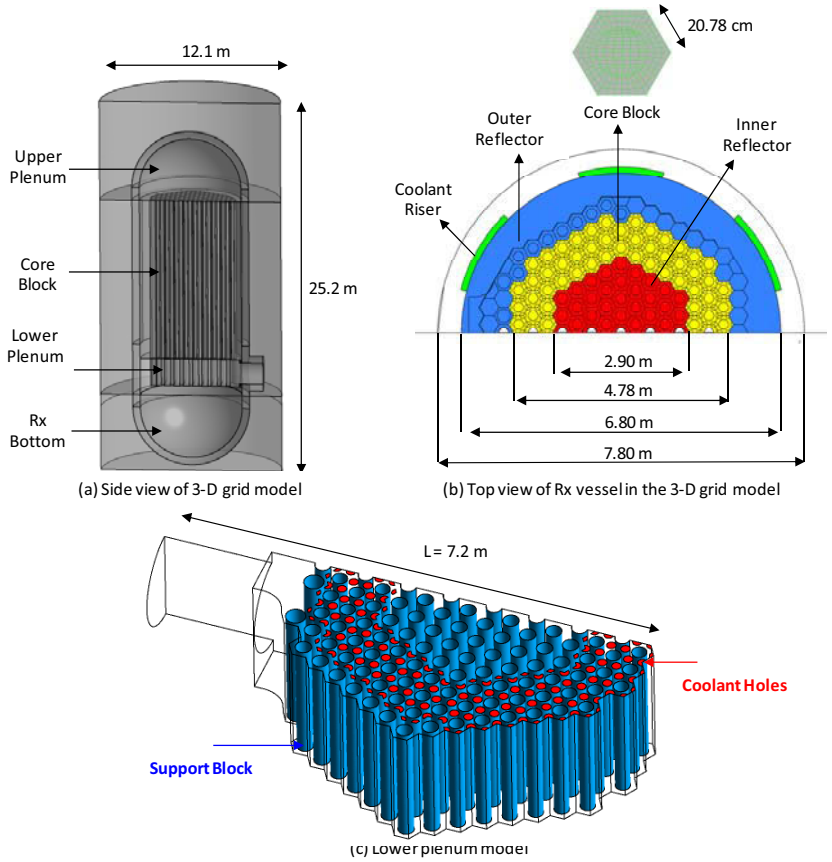

Figure 1. 3-D grid model for VHTR air-ingress accident.

Table 1. Number of mesh and volume data for each region in the 3-D grid model.

<table>
<tr><th colspan="2">Reactor Internal</th><th>Confinement</th></tr>
<tr><td>Core Blocks</td><td>- Volume : 60.35 m^3 (Volume Porosity : 0.185)
- Height : 10.82 m
- Hexahedral mesh : 2,248,560</td><td rowspan="5">- Volume : 961.05 m^3

- Hexahedral mesh : 621,183

- Fluid volume ration the confinement to the re actor internal : 3.81</td></tr>
<tr><td>Lower Plenum</td><td>- Volume : 15.29 m^3
- Height : 1.84 m
- Hexahedral mesh : 677, 917
- Tetra mesh : 25,940
- Pyramids mesh : 1,103</td></tr>
<tr><td>Upper Plenum</td><td>- Volume : 66.27 m^3
- Radius : 3.4 m
- Hexahedral mesh : 712,023</td></tr>
<tr><td>Coolant Riser</td><td>- Volume : 6.98 m^3 (2.328 $m^3 \times 3$)
- Height : 9.87 m
- Hexahedral mesh : 287,820 (2.328 $m^3 \times 3$)</td></tr>
<tr><td>Rx Bottom</td><td>- Volume : 82.33 m^3
- Hexahedral mesh : 651,963</td></tr>
<tr><td colspan="3">- Total meshes number : 8,517,835</td></tr>
</table>

Figure 2 shows the g eometry and the mesh of the 3-D grid model at the lower part of the reactor. As shown in this figure, all the meshes are finely distributed throughout the whole geometries. The supporting graphite rods in the lower plenu m were modeled as tho se of the GT-MHR. Because of the complexity of the pebble core or the prismatic core, the core region is simplified to be a porous bod y with a 0.2 volume porosity. The parameters related to the permeability were estimated based on the circular channel friction data which is reported by Oh et al. (2008). The 2 mm bypass gaps between the core blocks were also neglected to avoid large number of cells required.

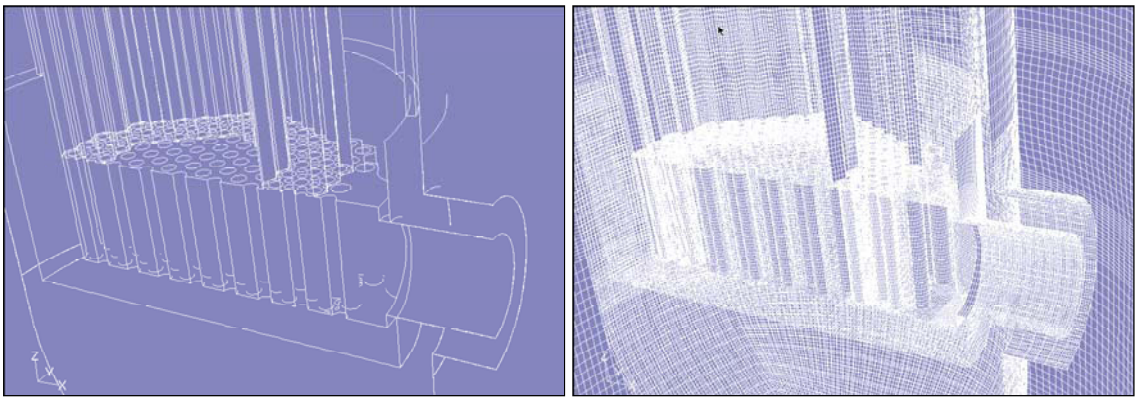

(a) Geometry (b) Mesh

Figure 2. Geometry and mesh of the 3-D grid at the lower part of the reactor.

Table 2 summarizes the reference model setup f or the CFD simulation. In this paper, FLUENT 6.3.26, a commercial CFD code was used for 3-D simulations which are based on the steady state calculations. Steady state calculations were made because we are interested in flow patterns. Since the temperature changes in the VHTR are relatively very slow because of large heat capacities of solid structures, the natural circulation phase can be assumed to be

quasi-steady-state. Parametric studies have been added to cover wide ranges of the conditions. Energy equation and species conservation equations were solved along with the realizable k-e model to be the reference viscous model. In the parametric studies, laminar, k-w, and RSM models were also taken into considerations. The density of the fluid was calculated by the incompressible ideal gas law, and the other properties were calculated by mixing laws. The multi-component diffusion model was selected for the diffusion coefficient, but this model does not affect the calculation results because the gas species are fully mixed in this modeling. The heterogeneous graphite oxidation was not considered in this modeling because of model complexities for this scoping analysis. The detailed effect of graphite oxidation on the air-ingress will be included in the near future when the VHTR conceptual design is finalized. The residuals of the simulation are determined to be 1e-4 for continuity, 1e-3 for momentum, 1e-6 for energy, and 1e-3 for k and epsilon.

Table 2. Reference FLUENT model set-up.

Parameters	Settings
Code Version	FLUENT 6.3.26
Solver Type	Pressure Based Solver
Time Scheme	Implicit
Dimension	3-D
Steady/Unsteady	Steady
Number of CPUs	20
Velocity Formulation	Absolute
Gradient Option	Node Based
Porous Formulation	Physical Velocity
Viscous Model	Realizable k-e
Pressure-Velocity Coupling	SIMPLE
Air Mass Fraction	0.5 (=0.12 for mole fraction)
Energy Equation Solve	Yes
Species Equation Solve	Yes
Density	Incompressible Ideal Gas Law
Heat Capacity	Mixing Law
Thermal Conductivity	Mass Weighted Mixing Law
Viscosity	Mass Weighted Mixing Law
Diffusion	Multi-component

Figure 3 shows the reference boundary conditions for the CFD simulation. The core temperature and the initial temperature of the air mixture following the depressurization were calculated from the GAMMA code (Oh et al. 2008, 2009) simulation. The distribution of the temperature was implemented into the core wall and the initial core temperature distributions. The reactor and the cavity side wall temperatures were assumed to be 763 K and 473 K for the base case. The lower plenum temperature was assumed to be 1145 K at the wall. Cavity top and bottom wall were assumed to be adiabatic. In the parametric studies, the effect of boundary temperatures on each part has been considered. Table 3 summarizes all the simulation cases and the conditions used for this study. The temperatures of the lower plenum were determined between about 945 K and 1145 K. These temperatures were based on the previous air-ingress simulation in the natural circulation phase. The air mass fraction was changed between 0.1 and 0.9 as shown in Table 3. It covers wide ranges of possible boundary conditions.

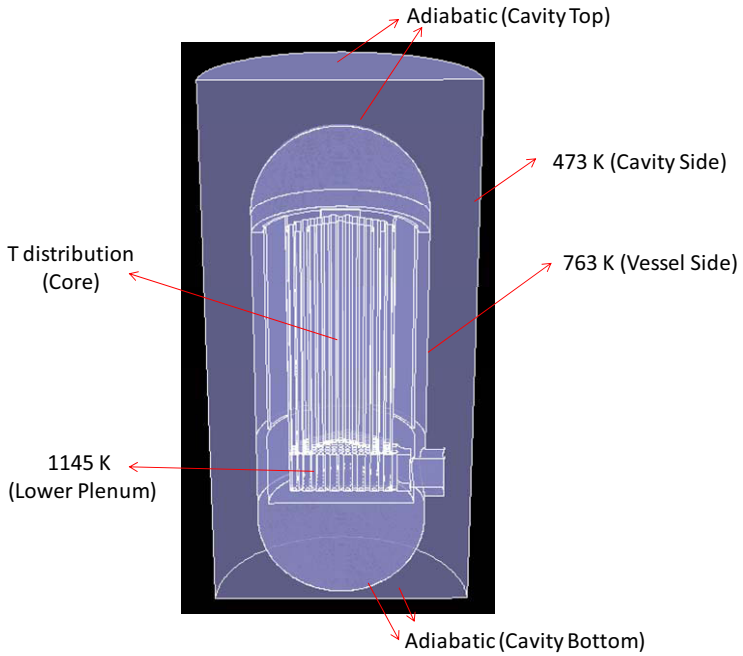

Figure 3. Reference boundary conditions for the CFD simulation.

Table 3. Simulation cases and conditions.

Case	Turbulence Model	Cavity Side Wall T (K)	Vessel Side Wall T (K)	Lower Plenum Wall T (K)	Air Mass Fraction
1 (base)	Realizable k-e	473	763	1145	0.5
2	Lam	473	763	1145	0.5
3	k-w	473	763	1145	0.5
4	RSM	473	763	1145	0.5
5	Realizable k-e	473	763	945	0.5
6	Realizable k-e	473	763	1045	0.5
7	Realizable k-e	373	763	1145	0.5
8	Realizable k-e	573	763	1145	0.5
9	Realizable k-e	473	763	1145	0.1
10	Realizable k-e	473	763	1145	0.9
11	Realizable k-e	473	663	1145	0.5
12	Realizable k-e	473	863	1145	0.5

3. RESULTSAND DISCUSSIONS

This section summarizes the CFD simulation results and discussion. Figures 4 through 7 show the calculation results for the base case (See Tables 2 and 3). In the base case, the realizable k-e model was selected to be a turbulence model. The cavity and the vessel wall temperatures were assumed to be 473 K and 763 K, respectively. The lower plenum temperature was set as 1145 K on the basis of the GAMMA code results for the depressurization phase. The core temperature was also obtained from the GAMMA code calculations. The air mass fraction of 0.5 which was used as an initial condition was calculated using the GAMMA code based on 25,000 m3 confinement volume in the GT-MHR design.

Figure 4 shows the contour plot of the temperature at the reactor cross-section. A notable thing in this figure is the thermal stratification showing up at the hot-leg and the lower plenum. In this figure, the left bottom is occupied with cold fluids (~ 540 K), and the right top with hot fluids (~1100 K). This temperature gradient provides very significant density gradient because the density of the gas is proportional to an inverse of the temperature. Figure 5 shows the density gradient at the reactor cross-section. As shown in this figure, there is a clear density change between hot and cold fluids along with the temperatures. This thermal stratification is originated from the temperature difference between inside and outside of the reactor vessel. In the inside of the reactor, the high temperature is maintained in the air-ingress accident because of the core decay heat and the resident heat in the solid structures. On the other hand, in the outside of the reactor, the relatively cold temperature is maintained because of the cavity cooling system.

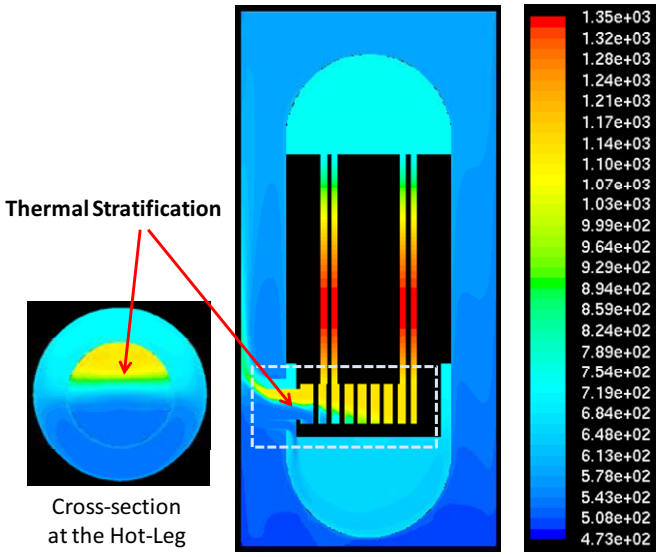

Figure 4. Temperature (K) contour plot (base case).

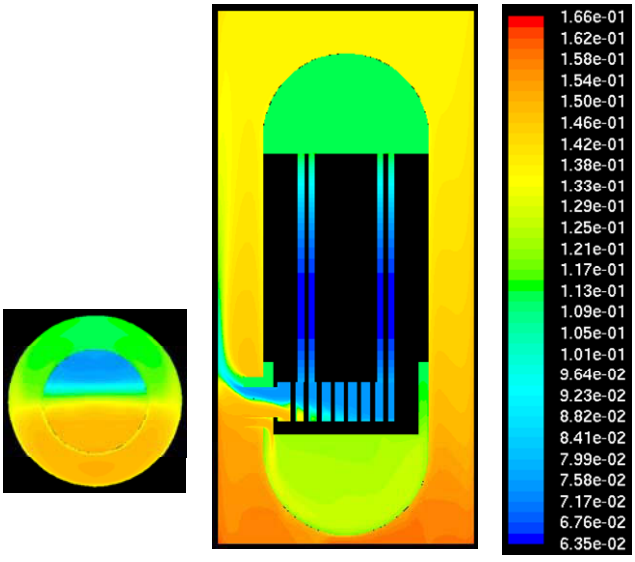

Figure 5. Density (kg/m^3) contour plot (base case).

The importance of this thermal stratification is that the density gradient by the temperature generates re-circulation flow thorough the hot-leg and the lower plenum. The basic principle of this phenomenon is exactly the same as the density gradient driven stratified flow between air and helium after the depressurization phase. The only difference is that the density gradient is contributed by non-uniform temperature distributions in this case. Figures 6 and 7 show the contour plots for the absolute and x-directional velocities, respectively. These figures show that the counter current is formed through the hot-leg to the lower plenum. In Figure 7, the blue color represents the flow into the reactor while the red color, the flow out of the reactor. The vector plot in the Figure 8 more clearly shows the re-circulation flow at the broken hot-leg. As shown in this figure, the cold fluids are coming into the reactor through the lower part, and the hot fluids are going out through the upper part. This re-circulation pattern is apparent and important, but it has never been seen in the previous air-ingress modeling results when the 1-D GAMMA code was used.

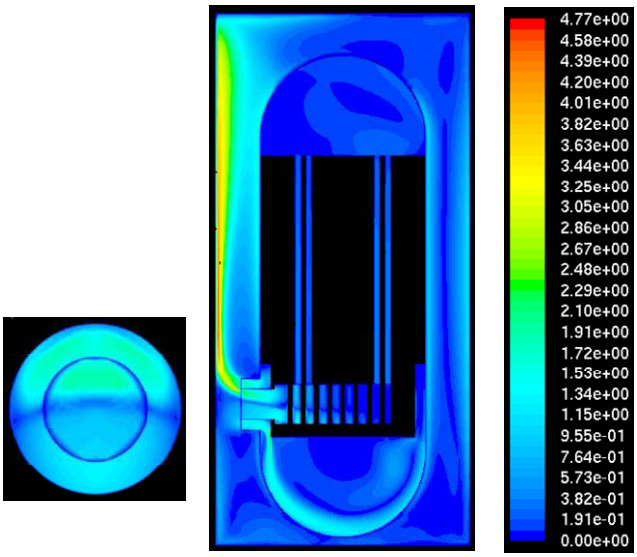

Figure 6. Velocity (m/s) contour plot (base case).

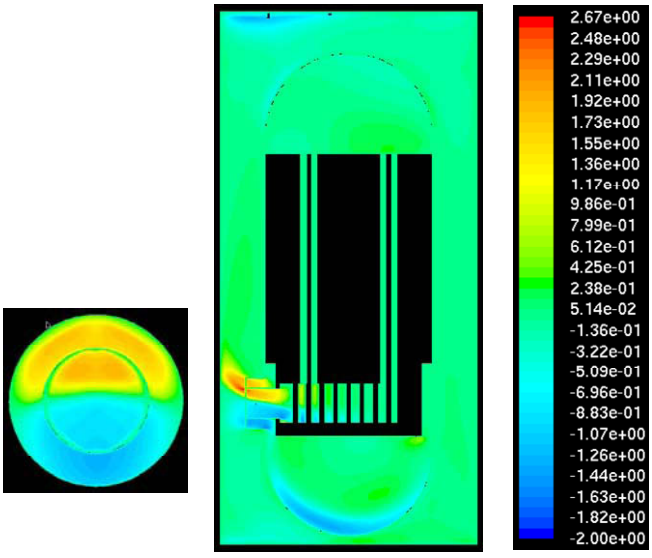

Figure 7. x-velocity (m/s) contour plot (base case).

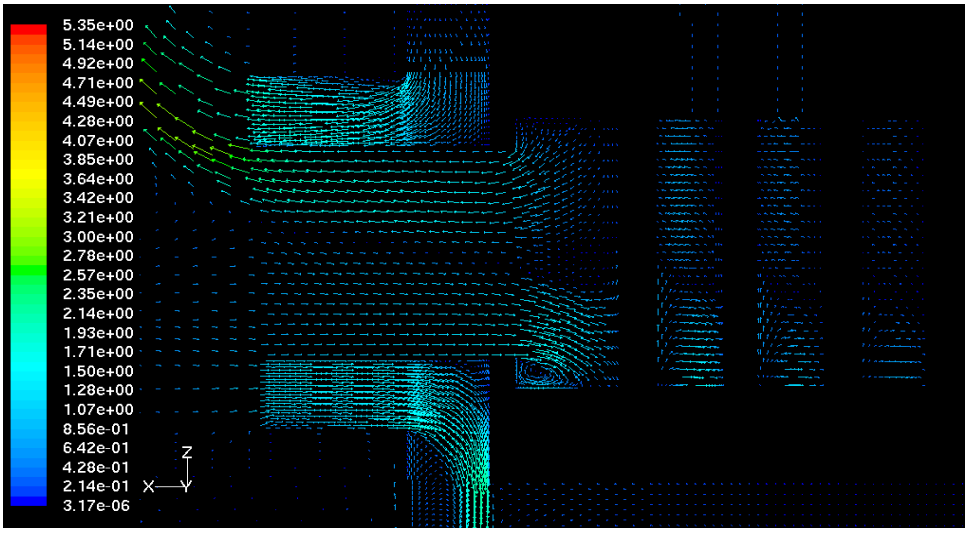

Figure 8. Velocity vector at the broken pipe (base case).

The existence of this re-circulation flow in the lower plenum is a very important issue because this different flow pattern may result in more aggressive graphite oxidation on the supporting graphite rods in the lower plenum. Figure 9 shows the comparisons of natural circulation patterns between the 1-D assumption and the 3-D simulation. The biggest difference between these two cases is the existence of the re-circulation flow as described above. As a result, the re-circulation flow will make the air-ingress accident more serious than predicted in the earlier studies.

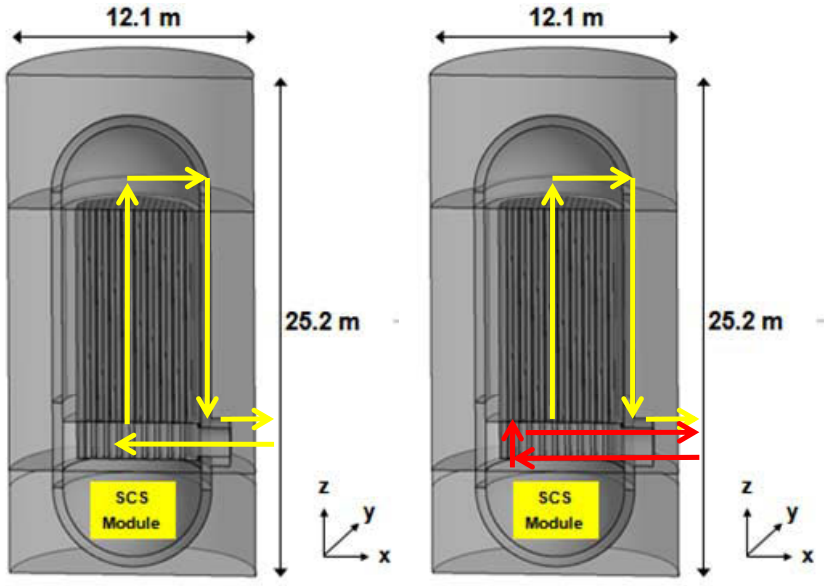

(a) 1-D assumption (b) Multi-D simulation

Figure 9. Comparisons of natural circulation flow patterns between 1-D assumption and 3-D simulation.

Figure 10 and Table 4 show why this re-circulation flow makes the air-ingress accident more serious. Figure 10 plots the x-velocity profile in the z-direction at the broken hot-leg. In this figure, the left-hand side is the hot-leg bottom and the right-hand side is the hot-leg top. The

positive (+) velocity represents the inward flow, and the negative velocity represents the outward flow. This figure clearly shows the counter current flow throughout the pipe. In this figure, the ingress speed of the cold fluid is ranged between 0 and 1 m/s. The maximum speed is 1.08 m/s, and the average speed is about 0.74 m/s. The superficial velocity, which is averaged by the whole pipe cross-sectional area, is 0.46 m/s. Table 4 summarizes the estimated air-ingress speeds for various conditions and assumptions. An important issue of the re-circulation flow is that the air-ingress speed is much faster than that predicted by the previous 1-D model. According to the previous GAMMA code calculation (Oh et al., 2008), the speed of the air-ingress through the broken pipe ranges between 0.03 ~ 0.05 m/s as shown in Table 4. It indicates that the air-ingress speed in the 3-dimensional simulation is about an order faster than the 1-D simulation. Therefore, in the real situation, the graphite in the lower plenum will be oxidized and corroded much faster than the previous predictions leading to more serious consequences. The re-circulation flow is also expected to change the graphite corrosion patterns in the support structures by different flow paths. For the natural circulation in the core, both 1-D and 3-D calculations showed very similar velocity values, which range between about 0.1 and 0.2 m/s.

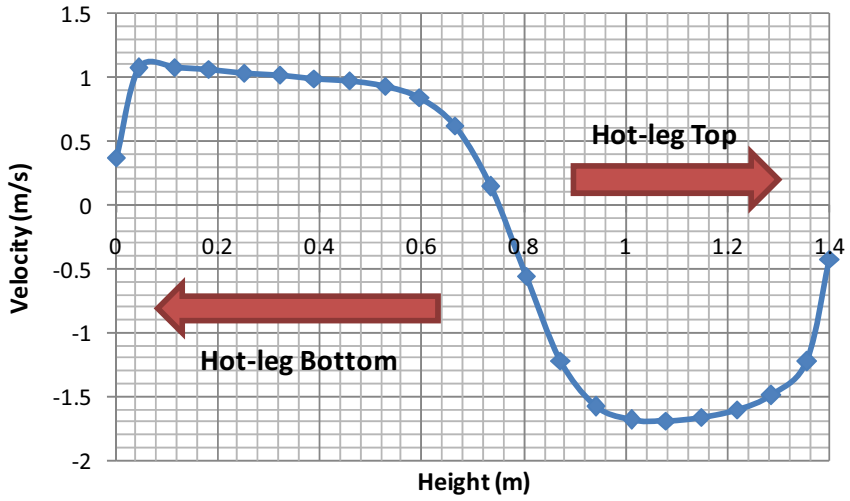

Figure 10. x-velocity profile at the broken hot-leg (base case).

According to Table 4, the air-ingress speed by re-circulation flow is not highly affected by the boundary conditions. For most of cases, the average velocity ranges between 0.7 ~ 0.75. In this parametric study, the temperature was selected within ± 100 K from the base case. The biggest difference was estimated by the air mass fraction changes. The increase of the air mass fraction clearly showed the increase of the air-ingress speed caused by the increase of driving force for the larger densities. In this study, the effect of turbulence models on the air-ingress speed was estimated to be very small. However, there are relatively large differences on the results between laminar and turbulence models. According to our calculations, the laminar model predicted larger air-ingress speed into the reactor. It is because the turbulence mixing effect reduces the temperature and density gradient in the flow, which is the driving force of the re-circulation flow.

Table 4. Estimated air-ingress speeds at the broken hot-leg.

	Average Speed (m/s)	**Maximum Speed (m/s)**	**Superficial Speed (m/s)**
1-D Modeling (GAMMA code)	0.03 ~ 0.05	0.03 ~ 0.05	0.03 ~ 0.05
Case 1 (base)	0.74	1.08	0.46
Case 2	0.80	1.00	0.48
Case 3	0.73	1.19	0.45
Case 4	0.73	0.98	0.45
Case 5	0.7	1.01	0.43
Case 6	0.73	1.07	0.45
Case 7	0.74	1.04	0.46
Case 8	0.75	1.05	0.47
Case 9	0.69	1.08	0.44
Case 10	0.88	1.07	0.51
Case 11	0.76	1.04	0.47
Case 12	0.71	1.07	0.45

4. SUMMARY AND CONCLUSIONS

In this paper, natural circulation patterns in the air-ingress accident conditions have been investigated using FLUENT, a commercial CFD code. The importance of the natural circulation pattern in the air-ingress accident is that it will significantly affect the predictions of the accident consequences including the graphite oxidation and corrosion-related problems.

The GT-MHR 600 MWt reactor was selected to be the reference design and modeled using a half symmetric 3-D geometry. The grid model was divided into six regions ((1) lower plenum, (2) core, (3) reactor top, (4) reactor bottom, (5) riser, (6) cavity), and merged by a grid interface function. In this model, the core was simply assumed to be a porous body with 0.2 volume porosity. The parameters related to the permeability were estimated based on the circular channel friction data. The 2 mm bypass gaps between the core blocks were also neglected to avoid large number of cells required. The simulation was the steady-state calculation. The following summarizes the notable results and conclusions.

The flow pattern that was visualized by the 3-D CFD simulation was quite different from the 1-D simple flow pattern, which was seen in the previous studies. In the 3-D simulation, the natural circulation is consisted of two flow paths. One is a normal natural circulation pattern through the core and the riser, and the other is the re-circulation pattern with a thermal stratification in the hot-leg and the lower plenum. The re-circulation pattern is very important because it is much faster than that predicted earlier by the 1-D simulations. The air-ingress speed by the re-circulation flow (~ 0.46 m/s in superficial velocity) is about an order magnitude faster than the 1-D calculations (0.02~0.03 m/s). It will result in much faster graphite oxidation and corrosion in the graphite supporter. The thermal stratification and the re-circulation pattern will eventually result in very complicated graphite oxidation and corrosion patterns. Further researches are planned in the near future. Therefore, the 3-D simulation indicates that the 1-D air-ingress modeling may significantly distort the air-ingress scenario and consequences.

All the results strongly recommend further researches on the thermal stratification phenomena and the re-circulation flow in the hot-leg and the lower plenum. Accordingly, validations of the CFD simulations on the key phenomena including density gradient driven flow are

currently in progress at Idaho National Laboratory to support the current computational studies.

ACKNOWLEDGMENTS

The submitted manuscript has been authored by a contractor of the U.S. Government through the Department of Energy's Nuclear Hydrogen Initiative and Power Conversion Program under DOE Idaho Operations Office Contract DE-AC07-051D14517. Accordingly, the U.S. Government retains a nonexclusive, royalty-free license to publish or reproduce the published form of this contribution, or allow others to do so, for U.S. Government purposes.

REFERENCES

1) ANSYS, ICEM CFD-11.0, Manual, 2008.
2) Johnson, R. W., Modeling strategies for unsteady turbulent flows in the lower plenum of the VHTR, *Nuclear Engineering and Design*, 238, pp. 482-491, 2008.
3) Kim, E.S., NO, H.C., Kim, B., and Oh, C.H., Estimation of Graphite and Mechanical Strength Variation of VHTR during Air-ingress Accident, *Nuclear Engineering and Design*, 238, 2007.
4) NO, H.C., Lim, H.S., Kim, J., Oh, C.H., Siefken, L., and Davis, C., Multi-component diffusion analysis and assessment of GAMMA code and improved RELAP 5 code, *Nuclear Engineering and Design*, 237, pp. 997-1008, 2007.
5) Oh, C. H., Davis, C., Siefken, L., Moore, R., NO, H. C., Kim, J., Park, G. C., Lee, J. C., and Martin, W. R., Development of Safety Analysis Codes and Experimental Validation for a Very High Temperature Gas-Cooled Reactor, Final Report, Idaho National Laboratory, INL/EXT-06-01362, March 2006.
6) Oh, C. H., Kim, E. S., NO, H. C., and Cho, N. Z., Experimental Validation of Stratified Flow Phenomena, Graphite Oxidation, and Mitigation Strategies of Air Ingress Accident, FY08 Report, Idaho National Laboratory, INL/EXT-08-14840, December 2008.
7) Oh, C. H., Kim, E. S., NO, H. C., and Cho, N. Z., Experimental Validation of Stratified Flow Phenomena, Graphite Oxidation, and Mitigation Strategies of Air Ingress Accident, FY09 Report, Idaho National Laboratory, INL/EXT-09-16465, December 2009.
8) Schultz et al., Next Generation Nuclear Plant Methods Technical Program Plan, INL/EXT-06-11804, Rev 0.26, September 2006.
9) Takeda T., Air Ingress Behavior during a Primary-pipe Rupture Accident of HTGR, JAERI-1338, Japan Atomic Energy Research Institute, 1997.
10) Takeda, T. and Hishida, M., Studies on Molecular Diffusion and Natural Convection in a Multicomponent Gas System, *International Journal of Heat and Mass Transfer*, Vol. 39, No. 3, pp. 527-536, 1996.
11) Takeda, T., Air Ingress Behavior during a Primary-pipe Rupture Accident of HTGR, JAERI-1338, Japan Atomic Energy Research Institute, 1997.
12) Yih, C.S., Dynamics of Nonhomogeneous Fluids, Macmillan, 1965.